Mn spin domains in highly photoexcited (Cd,Mn)Te/(Cd,Mg)Te quantum wells

M. G. Tyazhlov, V. D. Kulakovskii, and A. I. Filin

Institute of Solid State Physics, 142432, Chernogolovka, Russia

D. R. Yakovlev,* A. Waag, and G. Landwehr

Physikalisches Institut der Universität, Würzburg University, Würzburg 97074, Germany

Direct spin and energy transfer between a dense two-dimensional electron-hole (e-h) magnetoplasma and a Mn spin subsystem via spd exchange has been studied. Time-resolved photoluminescence spectra of the magnetoplasma excited by a powerful 10-ns laser pulse in a single $Cd_{0.97}Mn_{0.03}Te/Cd_{0.75}Mg_{0.25}Te$ quantum well have been investigated in magnetic fields $B \leq 14$ T at helium temperature. A giant asymmetry of the plasma spin splitting has been observed in the spectra of dense homogeneously photoexcited plasma at high magnetic fields. This asymmetry has been explained in terms of formation of a domain structure within the magnetic subsystem, i.e., spatial stratification into regions with different Mn-spin temperatures. The Mn spin domains result from the Mn spin heating due to the direct spin-spin sd exchange between hot carriers and Mn via effective spin-flip scattering of electrons with simultaneous spin-flip of Mn. During the Mn spin heating under quasistationary excitation, first the Mn spin fluctuations grow and spin domains form, then the spin domain's volume increases. The spin domain's formation occurs due to resonant spin-flip scattering with a characteristic time ~ 1 ns. The nonresonant Mn spin heating has been observed also with a characteristic time of $\simeq 10$ ns. [S0163-1829(98)09039-0]

I. INTRODUCTION

The distinguishing feature of $(A^{II},Mn)B^{VI}$ dilute magnetic semiconductors[1] (DMS) is the coexistence of three subsystems that interact with each other. There are carriers in valence and conduction bands, phonons, and magnetic Mn spin subsystem. The interaction between these subsystems has been addressed by a number of studies.[1–6] However the problem of direct spin and energy exchange between photoexcited carriers and Mn spin subsystem is still weakly investigated as theoretically as experimentally.

Mn ions have five noncompensated electron spins in the $3d^5$ shell and form diluted magnetic subsystems in DMS.[1] Magnetic properties of DMS have been studied extensively during the last decade. It has been found that the dd interaction between Mn ions is an antiferromagnetic exchange $J_{dd} < 0$ determined by their spins.[1] The interaction is most effective for the nearest neighbors $(-J_{NN} \sim 10$ K),[3] and it decreases very rapidly with increasing Mn-Mn distance $(-J_{NNN} \sim 1$ K).[3,7] At small Mn concentrations ($x \leq 0.5$), most Mn ions have no Mn neighbors in the nearest shells, and the Mn subsystem demonstrates paramagnetic properties. For example, at $x \sim 0.03$ the paramagnetic phase contains up to 75% of the Mn ions.[3] The nearest neighbors form antiferromagnetic couples with a nonmagnetic ground state under magnetic fields of up to ~ 12 T at helium temperatures.[3]

The magnetic subsystem interacts strongly with the carriers in the valence (pd) and conduction bands (sd exchange interaction). These interactions are also expressed in terms of spin-spin products and result in a giant spin splitting of band states in an external magnetic field.[1,8] They generate ferromagnetic corrections to the main Mn-Mn antiferromagnetic interaction and leads to formation of a magnetic polaron, i.e.,

ferromagnetic spin ordering in the volume enveloped by a carrier wave function.[2] In $Cd_{1-x}Mn_xTe$ crystals with $x < 0.05$, the magnetic polaron energy is small owing to the small Mn concentration,[4] and the Mn spin subsystem was shown to be homogeneous and paramagnetic.[1] Recent research has demonstrated, however, that the situation changes drastically if DMS is highly photoexcited—the inhomogeneous heating of Mn subsystem has been found.[6] The experiment has been carried out on samples with narrow (Cd,Mn)Te quantum wells (QW's), which gave us an opportunity to investigate magnetic phenomena at high concentrations of photoexcited carriers without a notable lattice overheat.[6,9,10]

Previous high-excitation studies of DMS QW's showed that the Mn spin heating is controlled by the sd exchange with photoexcited magnetoplasma and characteristic time of this heating lies in a nanosecond range.[6,11] Magnetoplasma was generated by picosecond laser pulses, and the Mn spin subsystem temperature was derived from the violet shift of the 0-0 transitions in the e-h magnetoplasma and/or of the magnetic exciton line in an external magnetic field. The formation of spatial Mn spin domains (SD) with an elevated Mn ion spin temperature was also suggested.[6,11] The SD's manifest themselves in experiment as coexistence of two highly different relaxation times $\tau_{loc} \sim 4$ ns and $\tau_{Mn} = 270$ ns of the exciton emission line shift.[6,11] The shorter time is detected in measurements of photoluminescence (PL) owing to annihilation of excitons generated by an intense pumping pulse and reflects exciton diffusion out of the hot SD's. The longer time corresponds to the Mn spin-lattice relaxation. It has been derived from the time dependence of the energy of excitons generated by weak probe laser pulses following the strong pumping pulse.

The subject of this paper is the energy and spin exchange
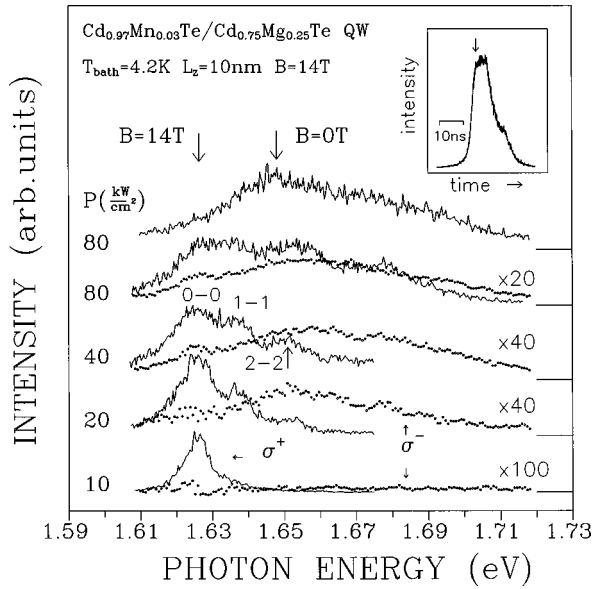
FIG. 1. Polarized σ^+ (solid line) and σ^- (dots) luminescence spectra from a single 10-nm $Cd_{0.97}Mn_{0.03}Te/Cd_{0.75}Mg_{0.25}Te$ QW recorded at various pulse excitation powers at $B=14$ T. The σ^- spectra are magnified for better viewing. The upper PL spectrum is recorded at $B=0$ and $P=80$ kW/cm^2. The arrows point to the free exciton positions at $B=0$ and $B=14$ T. The inset depicts the shape of the laser pulse and the time position of the light detector gate (the time gate width is 0.6 ns).

between the dense *e*-*h* plasma and the Mn ions in dilute magnetic $Cd_{0.97}Mn_{0.03}Te/Cd_{0.75}Mg_{0.25}Te$ QW under conditions of high quasistationary photoexcitation. The quasistationary regime allows us to detect PL from the SD and to investigate SD's time evolution.

The paper is organized as follows. The experimental technique is described in Sec. II. Section III describes experimental studies of magnetic-field-induced exciton spin splitting at low pumping powers. As was expected, the exciton spin splitting is symmetrical about its position at zero magnetic field. Peculiarities in the behavior of the $Cd_{0.97}Mn_{0.03}Te$ QW emission spectra with increasing excitation density are discussed in Sec. IV A. A giant asymmetry of the *e*-*h* plasma spin splitting has been detected, which indicates separation of the Mn spin subsystem into regions with low and high Mn spin temperatures (SD). The photoluminescence emitted immediately from SD's has been observed and the time evolution of SD's is described. Finally, in Sec. IV B, the experimental results are compared with theoretical predictions. It has been shown that spin-spin exchange interaction with *e*-*h* plasma results in spatial stratification of Mn spin subsystem.

II. EXPERIMENT

We have studied an undoped $Cd_{0.97}Mn_{0.03}Te/Cd_{0.75}Mg_{0.25}Te$ heterostructure with a single 10-nm-thick QW grown by the molecular-beam epitaxy on a (001)-oriented CdTe substrate. The sample was immersed in liquid helium in a cryostat with a superconducting coil. The QW plane was oriented normally to the magnetic field vector. Photoluminescence spectra were recorded at 4.2 K in the magnetic field range of 0–14 T using a grating monochro-
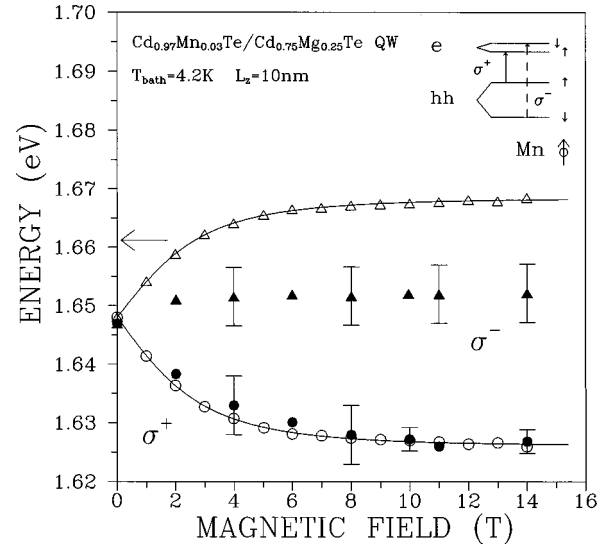
FIG. 2. Measurements of the transition energy for the plasma (full symbols) (pulse excitation $P=80$ kW/cm^2, $t=0$, PL) and for the free hh excitons (open symbols) (weak cw excitation, PLE) vs magnetic field measured at $T_{bath}=4.2$ K in σ^+ (circles) and σ^- (triangles) circular polarizations. The arrow points to the free lh exciton position at $B=0$ and $B=14$ T. At higher B the lh spin splitting does not exceed ~ 2 meV. The plasma energy was derived from the 0-0 transition at $B>10$ T and from the maximum of the PL line at $B=0$–10 T (Ref. 14). Solid lines plot the result of fitting using Eqs. (3.1) and (3.2), with $T_{Mn}+T_0$ as an adjustable parameter. The inset is a diagram of optically allowed transitions in external magnetic field.

mator and a time-correlated photon counting system (a time resolution of 0.3 ns). Nonresonant above barrier gap photoexcitation was produced by a Cu ion pulsed laser at a wavelength of 510 nm and a repetition rate of 10 kHz. The laser pulse had a trapezoid shape (see the inset in Fig. 1) with a characteristic rise time of about ~ 1 ns and a plane top width of about ~ 5 ns. Under such conditions, photoexcitation is quasistationary because the carriers lifetime does not exceed 0.5 ns.[12] A 0.6-mm optical fiber was used to provide a laterally uniform excitation and to collect the QW emission only from the homogeneously excited area of the sample.[9,10] A dedicated film analyzer located between the fiber and the sample was used to analyze circularly polarized PL components. The separation between the fiber and the sample was within 0.3 mm. The density of photoexcited carriers was determined by analyzing the plasma emission line shape.[9] It was up to $\sim 2 \times 10^{12}$ cm^{-2} at $W=80$ kW/cm^2. Photoluminescence excitation (PLE) spectra were recorded using a Ti-sapphire laser and a double grating monochromator.

III. EXCITON SPIN SPLITTING AT LOW cw EXCITATIONS

Magnetic field polarizes Mn spin subsystem in DMS. The edges of valence and conduction bands are spin split due to the *spd* exchange. A diagram of optically active transitions with σ^+ and σ^- circular polarizations in a magnetic field perpendicular to QW plane $B \| z$ is shown as an inset to Fig. 2. The magnetic field aligns Mn spins parallel to its direction, which is labeled by Mn↑ in Fig. 2. The heavy hole spin

in the σ^+ polarization is parallel to the Mn spin and to the spin of conduction electron Mn↑, hh↑, e↑)≡(hh↑, e↑) (in electron representation). The carrier spin alignment in the σ^- polarization is opposite (Mn↑, hh↓, e↓)≡(hh↓,e↓).

Figure 2 shows energies of excitons containing a light hole (lh) and a heavy hole (hh), $E_{h(l)h}$, versus magnetic field. In order to avoid the lattice overheat, the PLE spectrum was measured at a low cw photoexcitation density ~ 1 W/cm^2. The splitting between lh and hh in zero magnetic field equals ~ 13 meV. lh exciton has a mixed spin state and, as a consequence, almost does not split in magnetic field. The lh spin splitting does not exceed ~ 2 meV at $B = 14$ T. The splitting of the hh exciton in external magnetic field is the sum of the spin splittings in the valence and conduction bands (see the inset to Fig. 1). Heavy holes form pure spin states, and the magnetic-field-induced shift of the hh exciton is proportional to the average Mn spin $\langle S_z \rangle$, effective Mn concentration x^*, and the sum of the absolute values of the exchange integrals in the conduction $N_0\alpha$ and valence $N_0\beta$ bands:[1,8]

$$\Delta E_{hh}(B) = E_{hh}(B) - E_{hh}(0) = \pm \frac{1}{2}(|N_0\beta| + |N_0\alpha|)x^*\langle S_z \rangle.$$
$$(3.1)$$

Here $+$ ($-$) refers to σ^- (σ^+) circular polarizations, and N_0 is the number of unit cells per unit volume. The average Mn spin $\langle S_z \rangle$ is described by the Brillouin function for spin 5/2,[1,8]

$$\langle S_z \rangle = B_{5/2}\left(\frac{\mu_B g_{Mn} B}{k(T_{Mn} + T_0)} \right).$$
$$(3.2)$$

Here $B_{5/2}(y)$ is the Brillouin function, g_{Mn} is the g factor for Mn, μ_B is the Bohr magneton, k is the Boltzmann constant, T_{Mn} is the Mn spin temperature, T_0 is the phenomenological antiferromagnetic temperature suggested by Gaj *et al.*[8] to take into account the small Mn-Mn long-range interaction, and T_0 has an order of ~ 1 K for $x = 0.03$.[8] Equations (3.1) and (3.2) were suggested for bulk crystals,[8] but they also apply to QW's with widths sufficiently large to neglect the wave-function penetration into barriers.

Solid lines in Fig. 2 show the fitting to experimental data. As indicated by Eq. (3.1), the hh-exciton splitting is symmetrical about its zero-field position. The hh-exciton shift $\Delta E_{hh}(B)$ is large at $B < 6$ T. At higher B it increases relatively slowly and reaches $\Delta E_{hh} \sim 22$ meV at 14 T. The Mn spin temperature is close to the helium bath temperature $T_{Mn} + T_0 \simeq 5$ K, $T_{Mn} \simeq 4.2$ K. The measurements of the exciton shift and T_0 are in good agreement with those for bulk Cd$_{0.97}$Mn$_{0.03}$Te.[8]

IV. SPIN SPLITTING IN *e-h* PLASMA

A. Experimental results

Time-resolved PL spectra of a dense electron-hole (*e-h*) plasma in the σ^+ and σ^- polarizations at $B = 14$ T measured with a time gate of 0.6 ns are given in Fig. 1 for different excitation densities $P = 10$–80 kW/cm^2. The laser pulse intensity as a function of time is shown as an inset to Fig. 1. The arrow in the inset shows the time position of the
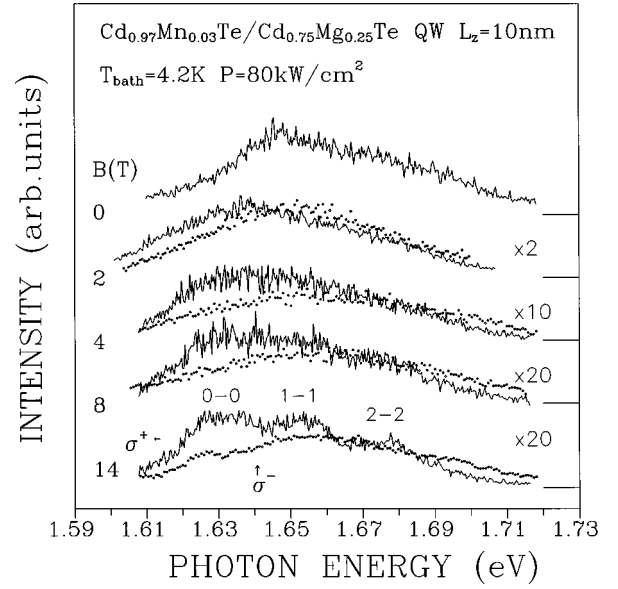
FIG. 3. Polarized σ^+ (solid line) and σ^- (dots) luminescence spectra from a single 10-nm Cd$_{0.97}$Mn$_{0.03}$Te/Cd$_{0.75}$Mg$_{0.25}$Te QW recorded at various magnetic fields at $P = 80$ kW/cm^2 and zero delay (the time gate width is 0.6 ns). The σ^- spectra are magnified for better viewing.

gate, which is hereafter referred to as delay $t = 0$. For comparison, Fig. 1 also shows a PL spectrum recorded at $B = 0$ and $P = 80$ kW/cm^2, which contains a broad band, whose width ~ 50 meV corresponds to the radiative recombination of a dense *e-h* plasma formed by electrons and heavy holes of the lowest subbands $n_z = 1$.[6,9,10] The analysis of the plasma line shape[13] yields the electron temperature $T_e \sim 300$ K.

The Mn spin subsystem polarizes as the magnetic field increases. Polarized luminescence spectra recorded at various magnetic fields at $P = 80$ kW/cm^2 and zero delay are given in Fig. 3. When magnetic field increases the PL line splits into two lines active in the σ^+ and σ^- polarizations, respectively. Figure 3 shows that the magnetic field behavior of the *e-h* plasma emission lines in σ^+ and σ^- polarizations is not similar to the case of the exciton spin splitting. This difference is also illustrated in Fig. 2, which shows the magnetic field dependence of the peak positions in the polarized PL spectra of excitons and of *e-h* plasma[14] at $P = 80$ kW/cm^2. It demonstrates that the magnetic-field dependence of the low-energy component of magnetoplasma σ^+ is rather similar to that of the exciton. Its line shift saturates in $B > 6$ T and equals ~ 20 meV at $B = 14$ T. The Mn spin temperature derived from this magnetic-field dependence is equal to $T_{Mn}^+ \cong 7$ K, which is close to T_{bath} and indicates a relatively small heating of Mn spins at $t = 0$. The high-energy component of the *e-h* magnetoplasma σ^- on the contrary, is almost independent of the magnetic field. An estimation based on Eqs. (3.1) and (3.2) yields the temperature $T_{Mn}^- \sim 200$–300 K. The difference between T_{Mn} derived from the σ^+ and σ^- circular polarizations indicates that $\langle S_z \rangle$ becomes essentially inhomogeneous.

Moreover, one can see in Figs. 1 and 3 that, as expected, the σ^+ polarization demonstrates at 14 T additional features related to the Landau quantization of the electron and hole
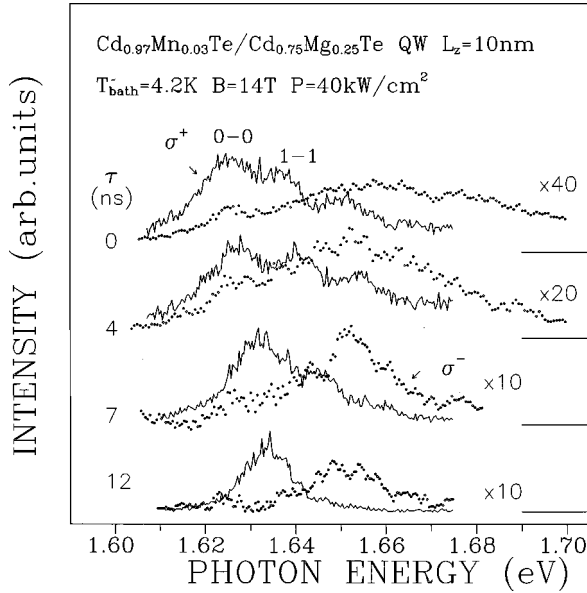
FIG. 4. Polarized σ^+ (solid line) and σ^- (dashed line) luminescence spectra from a single 10-nm $Cd_{0.97}Mn_{0.03}Te/Cd_{0.75}Mg_{0.25}Te$ QW recorded at $P=40$ kW/cm^2, $B=14$ T and various delays. The σ^- spectra are magnified for better viewing.

motion.[10] No features due to Landau levels (LL) have been detected in the σ^- polarization, although the halfwidth of the σ^- line is fairly large, ~ 50 meV, which exceeds the Landau-level spin splitting.

The σ^- line in the PL spectrum shows up only at high excitations, which can be seen by comparing PL spectra for $P=10$, 20, and 40 kW/cm^2 given in Fig. 1.

Figure 4 demonstrates evolution of PL spectra at $B=14$ T and $P=40$ kW/cm^2 for different delay times. In the range of quasistationary photoexcitation 0–5 ns, the PL spectra in the σ^+ polarization move monotonically to higher energies, which reflects the decrease in the average Mn spin $\langle S_z \rangle$ and the increase in the Mn temperature. The time dependence of the $\langle S_z \rangle$ and Mn spin temperature T_{Mn}^+ derived from the energy of the 0-0 transition in the σ^+ polarization are given in the inset to Fig. 5.[14] As it was mentioned above, at $t \sim 0$ ns, T_{Mn}^+ is close to the bath temperature. It increases with time and reaches ~ 20 K at $t \approx 5$ ns, which is still much smaller than the electron temperature $T_e \sim 100$ K.[13] The rate of the Mn spin heating $v_h = \Delta \langle S_z \rangle / \Delta t$ derived from measurements of the 0-0 transition at $P=40$ kW/cm^2 is $v_h \simeq -0.1$ ns^{-1} for the σ^+ polarization at $t=0$–5 ns. The Mn spin temperature T_{Mn}^- determined from the peak positions of PL line in the σ^- polarization is also plotted in Fig. 5. Figures 4 and 5 show that the energy of the σ^- component is almost independent of the delay and corresponds to T_{Mn}^- ~ 100–200 K.

Figure 5 also shows the integral intensity of the σ^+, I^+ and σ^-, I^- components of PL as functions of time. The curves of I^+ and I^- vs time are essentially different. The integral intensity I^+ follows the laser pulse intensity (compare with the inset in Fig. 1). Unlike the σ^+ polarization, the σ^- component appears in the PL spectra later. Under quasistationary excitation $t=0$–5 ns, the integral intensity I^-
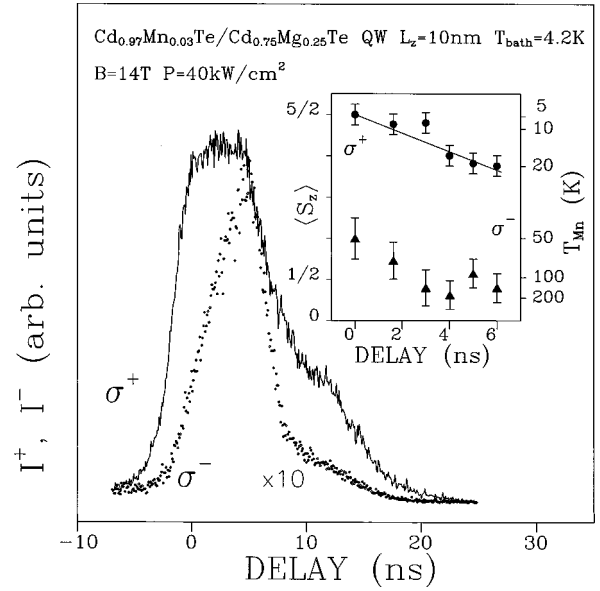
FIG. 5. Integral intensity of the σ^+ (I^+, solid line) and σ^- (I^-, dots) emission lines as functions of time at $P=40$ kW/cm^2 and $B=14$ T. The inset shows the averaged Mn spin and Mn spin temperature for σ^+ (circles) and σ^- (triangles) circular polarizations plotted against time under a quasistationary photoexcitation during $t=0$–6 ns. The solid line in the inset is a linear fitting of the Mn spin heating in the σ^+ polarization.

increases linearly with time. On the trailing edge of the laser pulse $t=5$–20 ns, the intensity I^- decreases faster than the laser pulse intensity.

B. Discussion

In nonmagnetic semiconductors photoexcited electrons and holes in semiconductors lose their energy to the phonon subsystem, which remains the only nonequilibrium subsystem after the carrier annihilation. In a DMS in an external magnetic field, there is another thermal reservoir. This is the subsystem of magnetic impurity spins, which interacts with both phonons and carrier spins. At helium temperatures, thermal equilibrium between phonons and Mn spins in $Cd_{1-x}Mn_xTe$ with $x=0.03$ is achieved after times of the microsecond range.[5]

Figures 4 and 5 demonstrate, however, very fast heating of the Mn spin subsystem taking a few nanoseconds. This time is two orders of magnitude shorter then the spin-lattice relaxation time. We ascribe this short time to direct energy transfer from the hot carriers to the magnetic subsystem of QW. This conclusion is also supported by our recent investigation of Mn spin heating in highly excited (Cd,Mn)Te QW's, when the independent control of the phonon subsystem has been carried out.[11]

Figure 1 shows that the 0-0 transition energy in the σ^+ polarization at $t=0$ increases little with the excitation density, which indicates that the Mn spin temperature T_{Mn}^+ remains close to T_{bath}. The magnetoplasma emission is expected to be 100% σ^+ polarized in the saturating magnetic fields even at $P=80$ kW/cm^2, because even in this case the hole Fermi energy E_{hh}^F does not exceed the valence band spin splitting ΔE_{hh}^s,[15] which is $\simeq 30$ meV. A relatively

weak and narrow σ^- band could be expected near ~ 1.67 eV due to recombination of thermally nonequilibrium holes. On the contrary, the emission spectra of magnetoplasma in Figs. 1 and 3 demonstrate a broad and rather strong feature at 1.65 eV. This can be explained only supposing intrinsic inhomogeneity of the Mn spin subsystem. The energy and spin transfer from the hot *e-h* plasma leads to spatial stratification within the Mn spin system into areas with relatively low (<30 K) and high (100–300 K) Mn spin temperatures.

Time evolution of hot and cold areas is also different. Figure 4 shows that the σ^+ spectrum shifts to higher energies during quasistationary excitation $t < 5$ ns. Such a shift means a decrease in $\langle S_z \rangle$ due to the increasing of Mn spin temperature. We estimate that at $B = 14$ T and $P = 40$ kW/cm^2 T_{Mn}^+ increases from ~ 5 K at $t = 0$ up to ~ 20 K at $t = 5$ ns. The σ^- radiation corresponds to a Mn spin temperature of about 100 K from the moment of its appearance in PL spectra. This temperature is close to the electronic one, whereas the integral intensity I^- increases with t. That indicates that the hot area volume increases during the excitation pulse. At $P = 40$ kW/cm^2 and $t = 5$ ns, I^-/I^+ equals about 10% (see Fig. 4). Under the highest excitation density (80 kW/cm^2, $t = 5$ ns) I^-/I^+ rises to $\sim 20\%$. This means that the hot areas can occupy up to 20% of the QW volume in our experimental conditions.

The Mn spin heating can be described by the following equation:

$$\Delta\langle S_z \rangle(t) = \langle S_z \rangle(t) - \langle S_z \rangle^* = \Delta\langle S_z \rangle_{\text{max}}(1 - e^{-t/\tau_{eMn}}). \tag{4.1}$$

Here τ_{eMn} is the characteristic time of the spin heating, $\langle S_z \rangle^* = 5/2$ corresponds to the Mn spin at $T_{\text{Mn}} = T_{\text{bath}}$ and $B = 14$ T, and $\Delta\langle S_z \rangle_{\text{max}}$ corresponds to the average Mn spin in thermal equilibrium between Mn spins and the electrons. As was mentioned above, at $P = 40$ kW/cm^2 the rate of Mn spin heating was $v_h \simeq -0.1$ ns^{-1} and $T_e \sim 100$ K. For this case, using Eq. (3.2), we can estimate $\Delta\langle S_z \rangle_{\text{max}} \simeq -2$ ($T_{\text{Mn}} \approx T_e$). By expanding Eq. (4.1) in powers of t/τ_{eMn}, we obtain $\tau_{eMn} \approx \Delta\langle S_z \rangle_{\text{max}}/v_h \sim 10$ ns.

The spin relaxation rate of an isolated spin due to the contact spin-spin interaction with spin-degenerate Fermi carriers, $1/\tau_{eMn}$, was considered by Abragam.[17] He carried out his calculations for spin 1/2 in a bulk crystal under conditions of thermal equilibrium in the electronic subsystem[18] and in sufficiently small magnetic fields, which allowed him to neglect the Landau quantization of electrons.

$$\frac{1}{\tau_{eMn}} = \frac{\pi}{\hbar}\alpha^2\rho(E_F^e)^2 kT_e. \tag{4.2}$$

Here $\rho(E_F^e)$ is the three-dimensional (3D) electron density of states on electron Fermi level E_F^e. The exchange constant in the conduction band α coincides with that in Eq. (3.1).

We have modified[11] these calculations for the discussed case of quasi-two-dimensional carriers and spin 5/2:

$$\frac{1}{\tau_{eMn}} = \frac{15\pi}{2\hbar}\alpha^2\left(\frac{D}{L_z}\right)^2 kT_e. \tag{4.3}$$

Here D is the 2D electron density of states. The increase of numerical coefficient reflects the growth of electron density of states in the 2D case and spin matrix element. For a high electron concentration, when the electron Fermi energy E_F^e exceeds the electron spin splitting ΔE_s^e, the spin relaxation rate turns out to be proportional to the electronic temperature, the density of states squared, and the interaction constant squared. Unlike the case of bulk crystals (4.2), τ_{eMn} in the 2D case is independent of the spin splitting and E_F^e position. This derives from the fact that the density of states is constant with the electron energy.

As was discussed in Sec. IV A, at $P = 40$ kW/cm^2 the electron temperature $T_e \simeq 100$ K. In the semiclassical approximation, neglecting the Landau quantization, we can estimate D as $D = 2 \times 10^{10}$ meV^{-1} cm^{-2} [$m_e = 0.096 m_0$ (Ref. 20)]. Using the values of T_e, D, and $\alpha = 1.5 \times 10^{-23}$ eV cm^3 [$N_0\alpha = 0.22$ eV (Ref. 8)] with Eq. (4.3) yields $\tau_{eMn} \sim 35$ ns for pumping $P = 40$ kW/cm^2. Therefore the calculations of τ_{eMn} are in reasonable quantitative agreement with the spin heating time $\tau_{eMn} \sim 10$ ns observed experimentally in the σ^+ polarization.

However, the above calculations cannot explain the high spin temperature T_{Mn}^- and the time evolution of σ^- spectra (see Fig. 4). Equation (4.3) was obtained in the approximation, which neglects the modulation of the electron density of states.[11] Obviously, this assumption does not hold at $B = 14$ T, when the optical spectra demonstrate a well pronounced Landau level structure (see Figs. 1, 3, and 4). The modulation of electron density of states must lead to an oscillating dependence of the spin relaxation rate on the electron spin splitting.[11] The parameter $1/\tau_{eMn}$ should demonstrate maxima under resonant conditions, when the electron spin splitting ΔE_e^s and the electron Landau splitting Δ_{0i}^e coincide:[21]

$$\Delta E_e^s = 0, \Delta_{01}^e, \ldots, \Delta_{0i}^e. \tag{4.4}$$

In our case of DMS we neglect the Mn spin splitting $\mu_B g_{\text{Mn}}B$ with respect to ΔE_e^s. The increase in $1/\tau_{eMn}$ in the resonant conditions (4.4), and the amplitude of the $1/\tau_{eMn}$ modulation $\Delta(1/\tau_{eMn})$ should be proportional to the inverse homogeneous linewidth Γ of the Landau levels:

$$\frac{\Delta(1/\tau_{eMn})}{1/\tau_{eMn}} \sim \int D^2 dE \sim \frac{\Delta_{01}^e}{\Gamma}. \tag{4.5}$$

The dependence of the spin relaxation rate on the electron spin splitting [Eqs. (4.4) and (4.5)] results in a positive feedback and can lead to the observed inhomogeneity of the Mn spin subsystem. From our point of view, the events develop according to the following scenario. There are two concurrent processes, namely, (i) the relatively slow Mn spin system heating as a whole due to the nonresonant spin-flip scattering and (ii) the fast heating of hot areas up to thermal equilibrium between Mn spins and electrons or up to the point where the resonant conditions (4.4) are satisfied. In our case, both of these conditions are approximately equivalent: $T_{Mn} \sim T_e \sim 100$–300 K $\leftrightarrow \Delta E_e^s \sim 0$.

On the first stage, with increasing of the laser pulse the electrons start to fill the excited spin level ($e\downarrow$) whereas the

holes in photoexcited magnetoplasma remain spin polarized (hh↑) because of much higher spin splitting.[15] The spin flip of the electrons from the spin-excited subband $e\downarrow$ results in the heating of the Mn spin subsystem due to $e\downarrow$ to $e\uparrow$ spin-flip processes with simultaneous spin-flip of Mn. The spin-flip of Mn increases the local spin temperature; therefore, it leads to a local decrease in the electron spin splitting. The local conditions of spin-flip scattering become closer to those of a resonance (4.4). This should result in an enhanced spin-flip scattering in these heated areas and in an enhancement in the Mn spin inhomogeneity. Therefore, the first stage of the Mn spin heating is controlled by Mn spin fluctuations and their time development.

The development of spin fluctuations up to saturation, i.e., up to $T_{Mn}\sim 100-300$ K proceeds very quickly within 1 ns. The hot areas manifest themselves as the σ^- PL band at the spectral position corresponding to the $T_{Mn}^-\sim 100$ K starting with $t=0$ (see Figs. 1, 3, and 4). Such a large difference between the nonresonant ~ 10 ns and resonant ~ 1 ns characteristic time of the Mn spin heating means that $\Delta(1/\tau_{eMn})\sim 1/\tau_{eMn}$. From Eq. (4.5) follows that in this case $\Gamma\sim\Delta_{01}^e$, which does not contradict our experimental results. Indeed, Figs. 1 and 3 show a well-resolved LL at $B=14$ T.

The characteristic properties of the hot spin areas allow us to classify them as spin domains. This term can be used, first, because of a very large temperature gradient at the boundary between the hot and the cold areas, and second, because of self-organization during the SD formation. The formation of SD ends the first fluctuation stage of Mn spin heating.

Then, on the second stage, the SD volume increases. This process is accompanied by increase in both the σ^- line intensity I^- and I^-/I^+ ratio, as can be seen in Fig. 5. The diffusion of hot Mn spins from the hot SD's to the cold areas via spin-spin relaxation plays an important role in this process so far as the spin-flip in the hot SD's is much faster. That is in agreement with the nanosecond order of magnitude for the spin-spin relaxation time known from the literature.[22,23] The spin diffusion results in an additional spin inhomogeneity and additional LL broadening as in σ^+ spectra due to the cold areas as well as in σ^- spectra due to the hot areas (see the absence of LL in σ^- spectra in Figs. 1, 3, and 4). After the end of the quasistationary excitation ($t>5$ ns), the relative intensity of σ^- line, I^-/I^+ decreases, which reflects the decrease in the electron density and the establishment of equilibrium within the Mn spin subsystem due to the spin diffusion.

V. CONCLUSION

The giant asymmetry of the plasma spin splitting has been observed in the range of high magnetic fields $B=10-14$ T in magnetoluminescence spectra of dense e-h plasma photoexcited in $Cd_{0.97}Mn_{0.03}Te/Cd_{0.75}Mg_{0.25}Te$ QW with a 10-ns laser pulse. We have demonstrated that the observed asymmetry is due to the development of spatial stratification within the magnetic subsystem in QW into areas with different spin temperatures. It occurs due to strong sd spin-spin interaction between Mn and hot e-h plasma. Development of Mn spin fluctuations leads to formation of Mn spin domains with a characteristic time of ~ 1 ns due to resonant spin-flip scattering. The nonresonant Mn spin heating has been observed also with a characteristic time of $\simeq 10$ ns. The photoluminescence emitted immediately from SD's has been observed.

---

*On leave from A. F. Ioffe Physico-Technical Institute, Russian Academy of Sciences, 194021 St. Petersburg, Russia.

[1] J. K. Furdyna, J. Appl. Phys. **64**, R29 (1988).

[2] P. A. Wolf, in *Semiconductors and Semimetals* (Academic Press, London, 1988), Vol. 25, p. 413.

[3] Y. Shapira, S. Foner, D. H. Ridgley, K. Dwight, and A. Wold, Phys. Rev. B **30**, 4021 (1984).

[4] D. R. Yakovlev and K. V. Kavokin, Comments Condens. Matter Phys. **18**, 51 (1994).

[5] T. Strutz, A. M. Witowski, and P. Wyder, Phys. Rev. Lett. **68**, 3912 (1992).

[6] V. D. Kulakovskii, M. G. Tyazhlov, A. I. Filin, D. R. Yakovlev, A. Waag, and G. Landwehr, Phys. Rev. B **54**, R8333 (1996).

[7] S. Nagata, R. R. Galazka, D. P. Mullin, H. Akbarzadeh, G. D. Khattak, J. K. Furdyna, and P. H. Keesom, Phys. Rev. B **22**, 3331 (1980).

[8] J. A. Gaj, R. Planel, and G. Fishman, Solid State Commun. **29**, 435 (1979).

[9] M. G. Tyazhlov, M. V. Lebedev, V. D. Kulakovskii, A. Forchel, D. R. Yakovlev, A. Waag, and G. Landwehr, Phys. Status Solidi B **188**, 565 (1995).

[10] V. D. Kulakovskii, M. G. Tyazhlov, A. F. Dite, A. I. Filin, A. Forchel, D. R. Yakovlev, A. Waag, and G. Landwehr, Phys. Rev. B **54**, 4981 (1996).

[11] M. G. Tyazhlov, A. I. Filin, A. V. Larionov, V. D. Kulakovskii, D. R. Yakovlev, A. Waag, and G. Landwehr, Zh. Éksp. Teor. Fiz. **112**, 1440 (1997) [Sov. Phys. JETP **112**, 830 (1997)].

[12] G. Mackh, W. Ossau, D. R. Yakovlev, A. Waag, G. Landwehr, R. Hellmann, and E. O. Göbel, Phys. Rev. B **49**, 10 248 (1994).

[13] V. D. Kulakovskii, E. Lach, A. Forchel, and D. Grützmacher, Phys. Rev. B **40**, 8087 (1989).

[14] In general, the maximum of the e-h plasma emission, as well as the energy of the 0-0 transition, does not coincide with the band gap edge because of broadening of the emission line and interparticle interaction (Refs. 1, 3, and 10). However, so far as we consider only the relative shift of the e-h plasma emission line in external magnetic field, this circumstance can be neglected.

[15] The sum of the bound states spin splitting, $\simeq 45$ meV at $B=14$ T and $T_{Mn}\sim T_{bath}$, is divided between the splittings in the conduction and valence bands in accordance, with the ratio between the exchange integrals (Ref. 8), $\Delta E_e^s\simeq 9$ meV and $\Delta E_{hh}^s\sim 36$ meV, i.e., the conduction-band splitting is much smaller than the hole one. On the contrary, the electron Fermi energy E_e^F is much larger than the hh Fermi energy E_{hh}^F because

$m_h/m_e \gtrsim 2$ (Ref. 16). As a result, even at $P=80$ kW/cm^2, when $E^F_{hh}+E^F_{hh}$ is up to 60 meV, $E^F_{hh} \lesssim 20$ meV, which is smaller then E^s_{hh}. Therefore, the holes should be highly spin polarized. In contrast, in the case of electrons, we have $E^F_e > \Delta E^s_e$ with a partial spin polarization of electrons at pumping power as low as $P \gtrsim 15$ kW/cm^2.

[16] L. C. Andreani, A. Pasquarello, and F. Bassani, Phys. Rev. B **36**, 5887 (1987).

[17] A. Abragam, *The Principles of Nuclear Magnetism* (Clarendon Press, Oxford, 1961), p. 334.

[18] In our case this assumption means that electron spin relaxation time should be shorter than ns scale, which has been recently supported by our experimental measurements of exciton spin relaxation time in similar Cd$_{0.88}$Mn$_{0.12}$Te/CdTe superlattice (10 nm/10 nm) (Ref. 19). Very short, about 5 ps characteristic time of exciton spin relaxation has been observed. This time becomes shorter when excitonic density increases. Thus, this assumption is in agreement with our experimental conditions.

[19] M. Tyazhlov, M. D. Martin, L. Vina, and L. L. Chang (unpublished).

[20] K. K. Kawasawa and F. C. Brown, Phys. Rev. **135**, 1757 (1964).

[21] Landau quantization of electron states leads to a dependence of the spin relaxation rate $1/\tau_{eMn}$ on the electron spin splitting because $1/\tau_{eMn}$ is proportional to the convolution between different spin subbands $\int D(E^e)D(E^e+\Delta E^e_s)dE$ (Ref. 11). As a consequence, $1/\tau_{eMn}$ must oscillate with the electron spin splitting ΔE^e_s with maxima at positions where the resonant conditions are satisfied [Eq. (4.4)].

[22] H. A. Sayad and S. Bhagat, Phys. Rev. B **31**, 591 (1985).

[23] R. E. Kremer and J. K. Furdyna, Phys. Rev. B **32**, 5591 (1985).